Highly birefringent chalcogenide optical fiber for polarization-maintaining in the 3-8.5 µm mid-IR window

Celine Caillaud,[1] Clement Gilles,[2] Laurent Provino,[3] Laurent Brilland,[3,4] Thierry Jouan,[1] Simon Ferre,[2] Mathieu Carras,[2] Mickael Brun,[2] David Mechin,[3] Jean-Luc Adam,[1] and Johann Troles[1,*]

[1]*Equipe Verres et Céramiques, ISCR UMR-CNRS 6226, Université Rennes 1, 35042 Rennes Cedex, France*
[2]*mirSense, 86 Rue de Paris, 91400 Orsay, France*
[3]*Perfos R&D, Platform of photonics Bretagne, 11 rue Louis de Broglie, Lannion, France*
[4]*SelenOptics, 263 Avenue Gal Leclerc, 35042 Rennes, France*
[*]*johann.troles@univ-rennes1.fr*

Abstract: A highly birefringent polarization-maintaining chalcogenide microstructured optical fiber (MOF) covering the 3-8.5 µm wavelength range has been realized for the first time. The fiber cross-section consists of 3 rings of circular air holes with 2 larger holes adjacent to the core. Birefringence properties are calculated by using the vector finite-element method and are compared to the experimental ones. The group birefringence is $1.5x10^{-3}$ and fiber losses are equal to 0.8 dB/m at 7.55 µm.

OCIS codes: (060.2420) Fibers, polarization-maintaining; (060.4005) Microstructured fibers; (060.2390) Fiber optics, infrared.

References and links

1. T. Hosaka, K. Okamoto, T. Miya, Y. Sasaki, and T. Edahiro, "Low-loss single polarization fibers with asymmetrical strain birefringence," Electron. Lett. **17**(15), 530–531 (1981).
2. R. D. Birch, D. N. Payne, and M. P. Varnham, "Fabrication of polarisation-maintaining fibres using gas-phase etching," Electron. Lett. **18**(24), 1036–1038 (1982).
3. R. B. Dyott, J. R. Cozens, and D. G. Morris, "Preservation of polarisation in optical-fibre waveguides with elliptical cores," Electron. Lett. **15**(13), 380–382 (1979).
4. A. Ortigosa-Blanch, J. C. Knight, W. J. Wadsworth, J. Arriaga, B. J. Mangan, T. A. Birks, and P. S. J. Russell, "Highly birefringent photonic crystal fibers," Opt. Lett. **25**(18), 1325–1327 (2000).
5. T. P. Hansen, J. Broeng, S. E. B. Libori, E. Knudsen, A. Bjarklev, J. R. Jensen, and H. Simonsen, "Highly birefringent index-guiding photonic crystal fibers," IEEE Photonics Technol. Lett. **13**(6), 588–590 (2001).
6. J. Ju, W. Jin, and M. S. Demokan, "Properties of a highly birefringent photonic crystal fiber," IEEE Photonics Technol. Lett. **15**(10), 1375–1377 (2003).
7. Y. Yue, G. Kai, Z. Wang, T. Sun, L. Jin, Y. Lu, C. Zhang, J. Liu, Y. Li, Y. Liu, S. Yuan, and X. Dong, "Highly birefringent elliptical-hole photonic crystal fiber with squeezed hexagonal lattice," Opt. Lett. **32**(5), 469–471 (2007).
8. T. Schreiber, F. Röser, O. Schmidt, J. Limpert, R. Iliew, F. Lederer, A. Petersson, C. Jacobsen, K. Hansen, J. Broeng, and A. Tünnermann, "Stress-induced single-polarization single-transverse mode photonic crystal fiber with low nonlinearity," Opt. Express **13**(19), 7621–7630 (2005).
9. K. Suzuki, H. Kubota, S. Kawanishi, M. Tanaka, and M. Fujita, "Optical properties of a low-loss polarization-maintaining photonic crystal fiber," Opt. Express **9**(13), 676–680 (2001).
10. J.-L. Adam and X. Zhang, *Chalcogenide Glasses* (Woodhead Publishing, 2014), Chap. 5.
11. P. Ma, D. Y. Choi, Y. Yu, X. Gai, Z. Yang, S. Debbarma, S. Madden, and B. Luther-Davies, "Low-loss chalcogenide waveguides for chemical sensing in the mid-infrared," Opt. Express **21**(24), 29927–29937 (2013).
12. P. Toupin, L. Brilland, C. Boussard-Plédel, B. Bureau, D. Mechin, J.-L. Adam, and J. Troles, "Comparison between chalcogenide glass single index and microstructured exposed-core fibers for chemical sensing," J. Non-Cryst. Solids **377**, 217–219 (2013).
13. U. Møller, Y. Yu, I. Kubat, C. R. Petersen, X. Gai, L. Brilland, D. Méchin, C. Caillaud, J. Troles, B. Luther-Davies, and O. Bang, "Multi-milliwatt mid-infrared supercontinuum generation in a suspended core chalcogenide fiber," Opt. Express **23**(3), 3282–3291 (2015).
14. W. Yuan, "2–10 µm mid-infrared supercontinuum generation in As_2Se_3 photonic crystal fiber," Laser Phys. Lett. **10**(9), 095107 (2013).

#259359 Received 12 Feb 2016; revised 16 Mar 2016; accepted 21 Mar 2016; published 5 Apr 2016

15. C. R. Petersen, U. Møller, I. Kubat, B. Zhou, S. Dupont, J. Ramsay, T. Benson, S. Sujecki, N. Abdel-Moneim, Z. Tang, D. Furniss, A. Seddon, and O. Bang, "Mid-infrared supercontinuum covering the 1.4–13.3 μm molecular fingerprint region using ultra-high NA chalcogenide step-index fibre," Nat. Photonics **8**(11), 830–834 (2014).
16. J. Troles, L. Brilland, F. Smektala, P. Houizot, F. Désévédavy, Q. Coulombier, N. Traynor, T. Chartier, T. N. Nguyen, J. L. Adam, and G. Renversez, "Chalcogenide microstructured fibers for infrared systems, elaboration modelization, and characterization," Fiber Integr. Opt. **28**(1), 11–26 (2009).
17. K. H. Tow, Y. Leguillon, S. Fresnel, P. Besnard, L. Brilland, D. Mechin, P. Toupin, and J. Troles, "Toward more coherent sources using a microstructured chalcogenide brillouin fiber laser," IEEE Photonics Technol. Lett. **25**(3), 238–241 (2013).
18. G. Ellis, G. Santoro, M. A. Gomez, and C. Marco, "Synchrotron IR microspectroscopy: Opportunities in polymer science," in *Synchrotron Radiation in Polymer Science* (IOP Publishing Ltd, 2010).
19. P. Hermann, A. Hoehl, G. Ulrich, C. Fleischmann, A. Hermelink, B. Kästner, P. Patoka, A. Hornemann, B. Beckhoff, E. Rühl, and G. Ulm, "Characterization of semiconductor materials using synchrotron radiation-based near-field infrared microscopy and nano-FTIR spectroscopy," Opt. Express **22**(15), 17948–17958 (2014).
20. E. Yoxall, M. Navarro-Cia, M. Rahmani, S. A. Maier, and C. C. Phillips, "Widely tuneable scattering-type scanning near-field optical microscopy using pulsed quantum cascade lasers," Appl. Phys. Lett. **103**(21), 213110 (2013).
21. M. Szpulak, J. Olszewski, T. Martynkien, W. Urbanczyk, and J. Wojcik, "Polarizing photonic crystal fibers with wide operation range," Opt. Commun. **239**(1-3), 91–97 (2004).
22. J. Ju, W. Jin, and M. S. Demokan, "Design of single-polarization single-mode photonic crystal fiber at 1.30 and 1.55 mu m," J. Lightwave Technol. **24**(2), 825–830 (2006).
23. B. Dabas and R. K. Sinha, "Design of highly birefringent chalcogenide glass PCF: A simplest design," Opt. Commun. **284**(5), 1186–1191 (2011).
24. S. Luke, S. K. Sudheer, and V. P. M. Pillai, "Modeling and analysis of a highly birefringent chalcogenide photonic crystal fiber," Optik (Stuttg.) **126**(23), 3529–3532 (2015).
25. M. Koshiba and K. Saitoh, "Applicability of classical optical fiber theories to holey fibers," Opt. Lett. **29**(15), 1739–1741 (2004).
26. M. Koshiba and K. Saitoh, "Finite-element analysis of birefringence and dispersion properties in actual and idealized holey-fiber structures," Appl. Opt. **42**(31), 6267–6275 (2003).
27. C. Caillaud, G. Renversez, L. Brilland, D. Mechin, L. Calvez, J.-L. Adam, and J. Troles, "Photonic bandgap propagation in all-solid chalcogenide microstructured optical fibers," Materials (Basel) **7**(9), 6120–6129 (2014).
28. D. Marcuse, *Light Transmission Optics*, (Van Nostrand Reihold Co, 1982).
29. H. G. Dantanarayana, N. Abdel-Moneim, Z. Q. Tang, L. Sojka, S. Sujecki, D. Furniss, A. B. Seddon, I. Kubat, O. Bang, and T. M. Benson, "Refractive index dispersion of chalcogenide glasses for ultra-high numerical-aperture fiber for mid-infrared supercontinuum generation," Opt. Mater. Express **4**(7), 1444–1455 (2014).
30. S. Legre, M. Wegmuller, and N. Gisin, "Investigation of the ratio between phase and group birefringence in optical single-mode fibers," J. Lightwave Technol. **21**(12), 3374–3378 (2003).
31. M. Antkowiak, R. Kotynski, T. Nasilowski, P. Lesiak, J. Wojcik, W. Urbanczyk, F. Berghmans, and H. Thienpont, "Phase and group modal birefringence of triple-defect photonic crystal fibres," J. Opt. A, Pure Appl. Opt. **7**(12), 763–766 (2005).
32. Z. Q. Tang, V. S. Shiryaev, D. Furniss, L. Sojka, S. Sujecki, T. M. Benson, A. B. Seddon, and M. F. Churbanov, "Low loss Ge-As-Se chalcogenide glass fiber, fabricated using extruded preform, for mid-infrared photonics," Opt. Mater. Express **5**(8), 1722–1737 (2015).
33. V. S. Shiryaev, M. F. Churbanov, G. E. Snopatin, and F. Chenard, "Preparation of low-loss core-clad As-Se glass fibers," Opt. Mater. **48**, 222–225 (2015).
34. Q. Coulombier, L. Brilland, P. Houizot, T. Chartier, T. N. N'guyen, F. Smektala, G. Renversez, A. Monteville, D. Méchin, T. Pain, H. Orain, J.-C. Sangleboeuf, and J. Trolès, "Casting method for producing low-loss chalcogenide microstructured optical fibers," Opt. Express **18**(9), 9107–9112 (2010).
35. K. Kikuchi and T. Okoshi, "Wavelength-sweeping technique for measuring the beat length of linearly birefringent optical fibers," Opt. Lett. **8**(2), 122–123 (1983).
36. J. Folkenberg, M. Nielsen, N. Mortensen, C. Jakobsen, and H. Simonsen, "Polarization maintaining large mode area photonic crystal fiber," Opt. Express **12**(5), 956–960 (2004).

1. Introduction

Polarization-maintaining fibers (PMFs) allow the propagation of optical signals with constant polarization all along the fiber. Advantages of PMFs are to minimize polarization mode dispersion and to eliminate polarization-dependent effects. These fibers could play an important role in integrated-optic devices, gas sensing application, interferometric techniques and high bit-rate transmission systems. Birefringence can be obtained by different ways. For example, the presence of mechanical stress within the cladding in the so-called PANDA [1] and/or bow-tie fibers [2] results in stress-birefringence. Also, fibers with elliptical core show form-birefringence [3].

#259359 Received 12 Feb 2016; revised 16 Mar 2016; accepted 21 Mar 2016; published 5 Apr 2016

Microstructured optical fibers (MOFs) provide new solutions for obtaining strong birefringence. Thus, high birefringence can be achieved by designing an asymmetric arrangement of air holes, where holes with two different diameters are placed along the orthogonal axes near the core region [4, 5]. This modification of the symmetry of the fiber structure results in a increase of the effective refractive index difference between the two orthogonal polarization modes. An asymmetric structure can be obtained in MOFs not only by altering the air holes size near the core area [4, 6], but also by changing the shape of air holes [7], or by introducing mechanical stress as demonstrated in [8]. It has been shown that the birefringence of silica polarization-maintaining microstructured optical fibers (PM-MOFs) can reach values of the order of 10^{-3}, which is one order of magnitude higher than that of PANDA or bow-tie silica fibers [9]. In this study, chalcogenide PM-MOF operating in the 3-8.5 μm infrared window is investigated for the first time.

Chalcogenide glasses are based on S, Se and/or Te associated with other elements like As, Ge, Sb and Ga. These glasses attract high interest because of their transparency in the infrared region [10]. Besides, the nonlinear refractive index (n_2) of chalcogenide glasses is 100-1000 times higher than that of silica glass at 1.55 μm, which makes them useful for nonlinear signal processing in optical communication systems. The optical guiding and dispersion characteristics of chalcogenide waveguides and fibers have been explored in recent years. These waveguides generate a great deal of interest in leading-edge research fields such as optical sensing [11, 12], supercontinuum generation [13–15], endlessly single mode fibers [16] or Brillouin fiber lasers [17]. In the mid-IR range, PMFs are of interest for devices where a broadband infrared source with high coherence and high brightness is utilized, as in surface plasmon resonance sensors or microscopes [18–20]. PMFs avoid the implementation of additional polarizing elements in optical systems, which would reduce the intensity of the IR signal and generate higher signal-to-noise ratio. Besides, to reduce the environmental instabilities due to mechanical vibrations and temperature variations of the source, a PMF can be used instead of a polarization controller coupled to a single-mode fiber.

In this study, a preliminary modeling is carried out in order to define the adequate optical geometry that permits polarization maintaining in a chalcogenide MOF. In a second step, a preform and a MOF presenting two larger holes in the first ring are prepared and drawn. Finally, the polarization maintaining behavior is studied, and birefringence measurements are performed and compared to results obtained by modeling.

2. Design and modeling of an ideal PM $As_{38}Se_{62}$ MOF

The schematic cross-section of studied PM-MOF is shown in Fig. 1(a). The microstructured cladding is composed of three rings of circular air holes forming a hexagonal lattice in a chalcogenide ($As_{38}Se_{62}$) glass background. This number of rings is sufficient to reduce the confinement loss, owing to high refractive index contrast between the core and the cladding. The birefringence into the MOF is induced by two larger holes adjacent to the fiber core, whose diameter (d_h) is greater than the diameter of the cladding air holes (d). The birefringence of silica PM-MOFs has been largely studied by varying the air-hole shapes and air-filling fractions in similar designs [9, 21, 22]. Recently, based on these studies on silica PM-MOF designs, chalcogenide PM-MOFs have been theoretically investigated [23, 24]. In this study, the hole-to-pitch ratio (d/Λ) and pitch (Λ) are fixed to 0.45 and 8 μm, respectively, which makes the PM-MOF single-mode over the 2-12 μm wavelength range [25]. The pitch value is also chosen large enough to better control the fabrication of the fiber with the molding and drawing method described in the next paragraph.

#259359 Received 12 Feb 2016; revised 16 Mar 2016; accepted 21 Mar 2016; published 5 Apr 2016

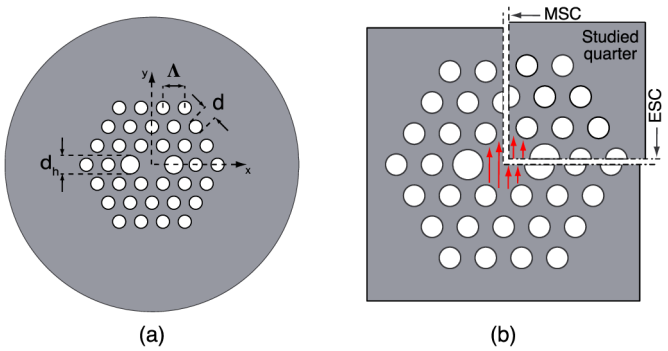

Fig. 1. (a) Schematic cross-section of PM-MOF. (b) MSC-ESC combination, applied on a quarter of a MOF, used to compute the y-polarized HE11 mode.

A full vector finite-element method (FEM), with circular perfectly matched layers as absorbing boundary conditions, is implemented to analyze the properties of the MOF. Because of the symmetry of the PM-MOF, only a quarter of the cross-section is used for the simulation and an electric or magnetic short circuit (ESC or MSC) is applied along each symmetry plane. ESC or MSC makes the electric field perpendicular or parallel to the boundaries, respectively. The polarization of a given mode over a quarter of the cross-section is preserved subject to the proper choice of a suitable combination of the two applied short circuits [26]. An example is given in Fig. 1(b) with the fundamental mode HE_{11} and a vertical-horizontal ESC-MSC combination. The wavelength-dependence of the background refractive index is also taken into account in the simulation. Therefore, a Sellmeier model is determined for fitting the refractive index values of $As_{38}Se_{62}$ chalcogenide glass, previously measured over the entire wavelength range 1.54-12 µm [27]. The fitting accuracy should be the dominant consideration in choosing a Sellmeier model. From the different tests conducted using a linear least-square fitting algorithm, we can conclude that a two-term Sellmeier model is a sufficient and unique model to represent accurately the refractive index of $As_{38}Se_{62}$ chalcogenide glass across this transparent window. The Sellmeier equation is of the form [28]

$$n^2(\lambda) = A_0 + \frac{A_1\lambda^2}{\lambda^2 - a_1^2} + \frac{A_2\lambda^2}{\lambda^2 - a_2^2}. \quad (1)$$

where A_0, A_1 and A_2 are dimensionless coefficients; a_1 and a_2 are the material resonant wavelengths and λ is the wavelength. The a_1 coefficient is associated with the optical bandgap absorption in visible/near-infrared regions, whereas a_2 is associated with vibrational band resonant absorption in the far-infrared region [29]. The values obtained for the coefficients are: $A_0 = 3.7464$, $A_1 = 3.9057$, $A_2 = 0.9466$, $a_1 = 0.4073$ µm and $a_2 = 40.082$ µm. The quality of fit is determined by the values of the summed squares of residuals and the root mean squared error, which are equal to $5.871\text{x}10^{-7}$ and $2.31\text{x}10^{-4}$, respectively. The refractive index of the air holes is set to 1.

Contrary to standard optical fibers, all modes in a MOF with a finite number of air-hole rings are inherently leaky because the core index is the same as the index of the outer cladding region without air holes. So, it has been verified that the higher-order modes have confinement losses greater than the HE_{11} modes over the studied wavelength range. The confinement losses of second-order modes are 6 or 7 orders of magnitude larger than those of HE_{11} modes. Therefore, the PM-MOF is supposed to be single-mode and the birefringence is calculated for the HE_{11} modes only. In Figs. 2(a) and 2(b), both the phase birefringence B and group birefringence B_g are represented, for three different values of d_h/Λ ratio. The phase birefringence is defined as $B(\lambda) = (n_y(\lambda) - n_x(\lambda))$, where n_x and n_y are the effective indices of

#259359 Received 12 Feb 2016; revised 16 Mar 2016; accepted 21 Mar 2016; published 5 Apr 2016

x-polarized HE_{11} mode (slow axis) and y-polarized HE_{11} mode (fast axis), respectively. The group birefringence is calculated from usual equation:

$$B_g(\lambda) = B(\lambda) - \lambda \frac{dB(\lambda)}{d\lambda}. \quad (2)$$

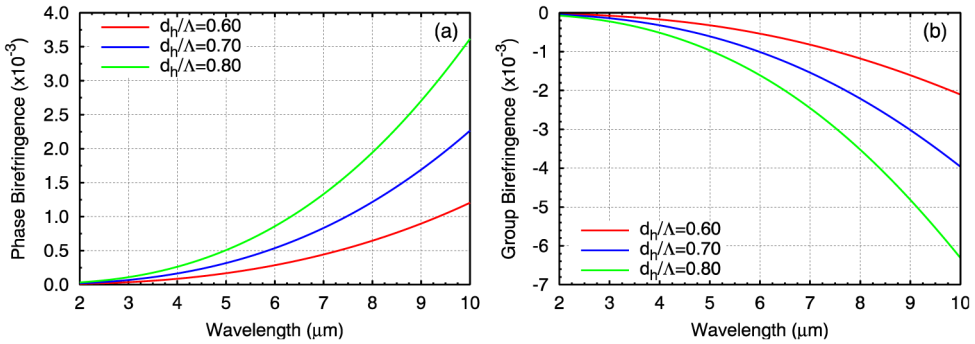

Fig. 2. (a) Phase birefringence and (b) group birefringence as a function of wavelength from 2.0 to 10.0 μm and for different values of d_h/Λ ratio. (The hole-to-hole pitch Λ is fixed at 8.0 μm).

All birefringence curves in Fig. 2 vary monotonically as wavelength increases. As expected, the phase birefringence increases with the d_h/Λ ratio. This is because increasing the d_h/Λ ratio further increases the difference between the effective indices of y and x-polarization modes. For wavelengths lower than 6 μm, the phase birefringence is similar to that of the conventional stress-induced birefringence fibers (10^{-4}), when the d_h/Λ ratio is 0.80. So, at these wavelengths, the beat length ranges from 1 cm to 6 cm, which is an order of magnitude over that of silica PM fibers. Moreover, this type of PM-MOFs can achieve phase birefringence values of the order of 10^{-3} for wavelengths greater than 6 μm. Regarding the group birefringence, one can observe that its absolute value is approximately twice as large as that of phase birefringence, with an opposite sign. This is typical of fibers that show significant contributions of form birefringence with normalized-frequency dependence [30, 31].

3. Fiber fabrication

The chalcogenide glass is elaborated from the $As_{38}Se_{62}$ glass composition. It is prepared by the conventional melt-quenching method by, first, introducing high purity As (99.999%), Se (99.999%) and $TeCl_4$ (99%) in a silica tube, which is then pumped under vacuum for 3 h [32, 33]. Further, the silica ampoule is sealed and placed in a rocking furnace at 850 °C during 12 hours to homogenize the melt. Addition of $TeCl_4$ to the raw starting elements permits the capture at high temperature of remaining hydrogen and carbon by forming HCl and CCl_4. Next, the mixture is cooled down to 700°C, quenched into water by immersion of the ampoule and annealed above the glass transition temperature T_g. Then, the chalcogenide glass rod, obtained after opening the ampoule, is placed into a distillation tube to be purified by several distillation steps. It is first distilled under dynamic vacuum to eliminate the low vapor pressure impurities such as carbon tetrachloride and HCl residues. In the second step, a distillation under static vacuum permits the elimination of refractory impurities, such as carbon, silica and other refractory oxides. When the distillation process is complete, the glass is further homogenized at 850 °C for 10 hours, cooled to 550 °C, quenched by immersion of the ampoule in water, and annealed above T_g to remove mechanical constraints.

The 3-ring microstructured preform shown in Fig. 3(a) is obtained by the molding method [34]. Briefly, this method consists in heating up the highly-purified glass rod obtained above

#259359 Received 12 Feb 2016; revised 16 Mar 2016; accepted 21 Mar 2016; published 5 Apr 2016

and in letting it flow into a silica mold whose design corresponds to the negative shape of the final preform. Both the glass rod and the silica mold are placed in a silica ampoule. The chalcogenide glass is flow down in the mold at 600 °C, which corresponds to a glass viscosity about 10^{-4} Pa.s. The mold is made of silica-glass capillaries organized in a hexagonal periodical pattern, which is implemented by using slices of a silica microstructured preform. The holes diameter is 460 µm (d) and the pitch is 1350 µm (Λ). In the present case, the geometry of slices is modified by placing two larger holes of 650-µm diameter in diametrically-opposed positions on the first ring, while respecting the d_h/Λ ratio. The thickness of the silica capillaries is about 30 µm. After the air quenching of the preform, the silica capillaries embedded in the chalcogenide preform were removed by a hydrofluoric acid treatment (10% of concentration). The diameter of the preform is typically of 16 mm with a length of 80 mm.

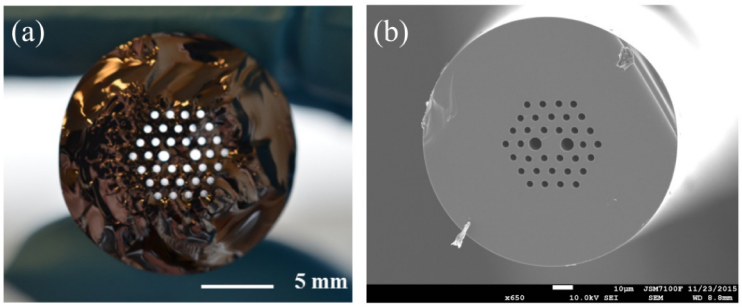

Fig. 3. (a) $As_{38}Se_{62}$ preform, and (b) Scanning electron microscope image of the $As_{38}Se_{62}$ MOF.

For drawing, the preform is installed in a silica enclosure under helium flowing to obtain an inert environment around the glass and to avoid any traces of moisture in the enclosure. Then, the lower extremity of the preform is heated above the softening point thanks to an annular electrical furnace. This results in the formation of a glass drop that falls under the gravitational force, which causes fiber drawing. Next, the fiber is attached to a rotating drum, and at the same time, the preform is translated down, feeding gradually the annular furnace. The fiber diameter is controlled by the translation speed of the preform and the rotation speed of the drum. During fiber drawing, the hole diameters are controlled by applying an inert gas (He) pressure in the holes of the preform. Any differential pressure is used during the drawing indeed the same pressure is applied into the different holes of the prefom

The obtained fiber has an outer diameter of 125 µm and a central solid core of 9 µm. Figure 3(b) shows a scanning electron microscope image of the fiber. Holes surrounding the core have a pitch of 7.64 µm and diameters of 3.46 µm for the small holes and 6.43 µm for the large ones. Light propagation is demonstrated with injection of monochromatic light at 3.39 µm from a He-Ne laser. The near-field image and 3D-profil at the output of the fiber are visualized with an infrared camera. They are represented in Figs. 4(a) and 4(b) respectively. The field distribution can be approximated by a Gaussian function in all directions, which indicates a single mode behavior at 3.39 µm. Consequently, a single propagation is expected within the transmission range of the fiber. One can note that the Gaussian output profile doesn't change whatever the bending of the tested fiber.

#259359 Received 12 Feb 2016; revised 16 Mar 2016; accepted 21 Mar 2016; published 5 Apr 2016

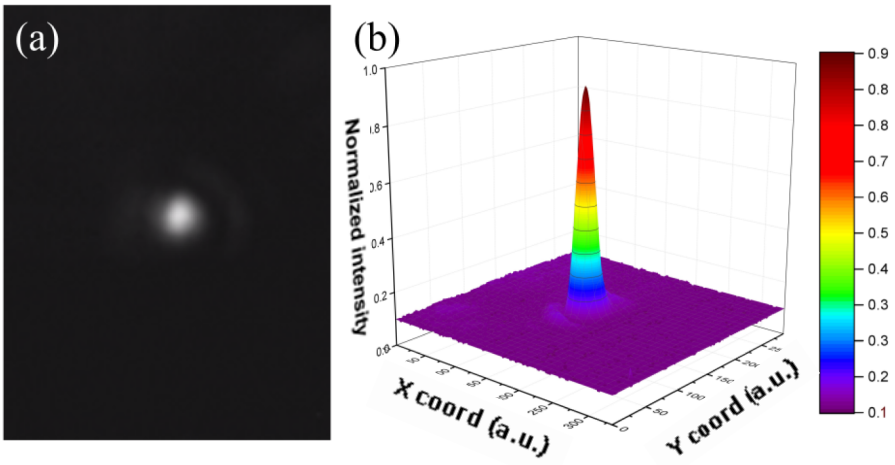

Fig. 4. (a) near field observation of 3.39 µm beam at the output of the AsSe MOF, and (b) 3D-representation of the near-field intensity distribution.

The optical losses of the MOF are measured with a Bruker Tensor 37 FTIR apparatus equipped with a cooled MCT detector. The attenuation of the PM-MOF, determined by the standard cut-back technique, is shown in Fig. 5. To obtain the optical losses of the core of the MOF, a GaSn alloy is applied on the surface of the fiber to inhibit cladding mode guidance. The PMF transmits light between 2 and 8.5 µm with a minimum of attenuation of about 0.3 dB/m at 6 µm. The attenuation curve presents extrinsic absorption bands at 2.9 µm, 4.26 µm, and 6.3 µm attributed to the presence of O-H groups, and of CO_2 and H_2O molecules, respectively. Besides, the optical losses at 1.55 µm are measured to be around 0.9 dB/m.

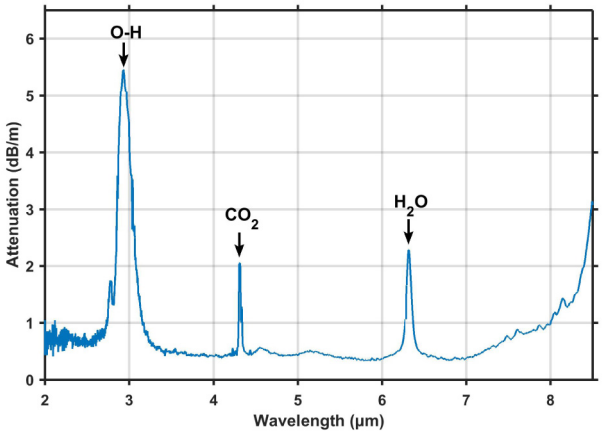

Fig. 5. Optical losses of the core of the PM-MOF.

4. Computation and measurements of the birefringence

The cross-section of the manufactured PM-MOF is displayed in the SEM picture of Fig. 6(a). The visual analysis shows some imperfections in the structure, which are produced during the fabrication processes. These small irregularities, such as the variation of the hole size and/or position, or the slight distortion of their shape, break the two-fold symmetry of the ideal fiber structure. The total birefringence is thus the combination of the birefringence due to the presence of two air holes with large diameters near the core region and that due to the imperfections related to each hole. To estimate as accurately as possible the birefringence of this fiber, it is necessary to carry out the real-model simulation. Therefore, we applied the full

#259359 Received 12 Feb 2016; revised 16 Mar 2016; accepted 21 Mar 2016; published 5 Apr 2016

vector FEM to a full structure, referred to as the "mask", deduced from the SEM picture of the manufactured fiber.

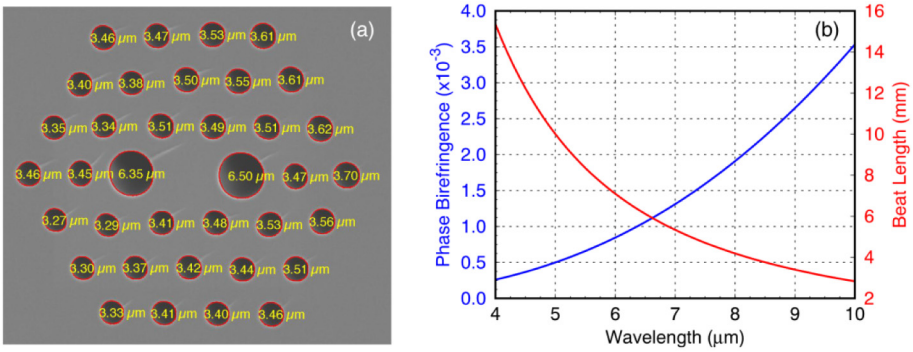

Fig. 6. (a) SEM picture of the manufactured PM-MOF with the boundaries and the mean diameter values of the air holes deduced from image processing. (b) Phase birefringence and beat length of the manufactured PM-MOF as a function of wavelength from 4 to 10 µm.

In this picture, the air holes appear in dark and the chalcogenide glass is in light grey. By means of a numerical treatment that consists in comparing the darkness of each point of the SEM picture to a decision level determined in the gray-scale, the boundaries, the size and the position of each air hole can be determined accurately. In Fig. 6(a), both the boundaries and the mean diameter values of the air holes deduced from image processing are indicated. The mean geometrical parameters d_h, d and Λ deduced from those measured from the SEM picture are equal to 6.43 µm (d_h/Λ = 0.84), 3.46 µm (d/Λ = 0.45) and 7.64 µm, respectively. These experimental geometrical parameters are quite close to those targeted (ratio d/Λ = 0.45 and Λ = 8.0 µm). Each hole and the surrounding chalcogenide region are then split in a mesh of triangular elementary subspaces, with dimensions small enough to describe properly the irregularities of each domain. Typically, the dimensions of these elements are chosen to be equal to $\lambda/10$ in the regions where the electric field is expected to be high, i.e. from the center to the first ring of holes, and it is equal to $\lambda/7$ elsewhere. Finally, the effective refractive indices of the two orthogonal polarization modes HE_{11} are computed by solving the Maxwell equations at each node of the grid and the total phase birefringence B is simply deduced. The obtained results are represented in Fig. 6(b). In order, to obtain a "mask" giving a proper description of the cross-section of the manufactured fiber, it is necessary to avoid any parallax error when taking the picture and to choose the proper decision level when operating its numerical treatment. The influence of a realistic change in this decision level on the computed total phase birefringence can be investigated by means of FEM analysis. The maximum uncertainty due to the numerical treatment of the picture is evaluated to be 5%.

The phase birefringence of an optical fiber is generally deduced from the measurement of the beat length. Different methods, such as the measurement of the polarised transversally diffused signal [35], the polarization time-domain reflectometry method [36] or the magneto-optical method are available. However, they are either very difficult to implement or they cannot be applied to highly birefringent fibers with a beat length as short as few mm. In this study, the group birefringence of the manufactured PM-MOF is determined by using the so-called crossed-polarizer technique [35]. Linearly polarized light is launched into a fiber of length L with the polarization oriented at 45 degrees with respect to the polarization axis of the fiber. At the fiber output, a polarizer is oriented at 45 degrees with respect to the polarization axis of the fiber and the spectrum is analyzed by Fourier Transform Infrared spectrometry with a resolution of 0.25 cm^{-1}. The optical sources used for the measurement are transverse magnetic polarized Fabry-Pérot Quantum Cascade Lasers (FP-QCL) operating at 5.25 µm, 5.55µm, 7.55µm and 8.2µm. The gain bandwidths of each laser are broad enough to

#259359 Received 12 Feb 2016; revised 16 Mar 2016; accepted 21 Mar 2016; published 5 Apr 2016

cover several phase oscillation periods. In Fig. 7, typical spectra are shown for a fiber of length L = 2.6 m at short and long wavelengths. Fiber length and spectrometer resolution are chosen with care to observe enough oscillations within the laser spectral width and to completely resolve the phase oscillations.

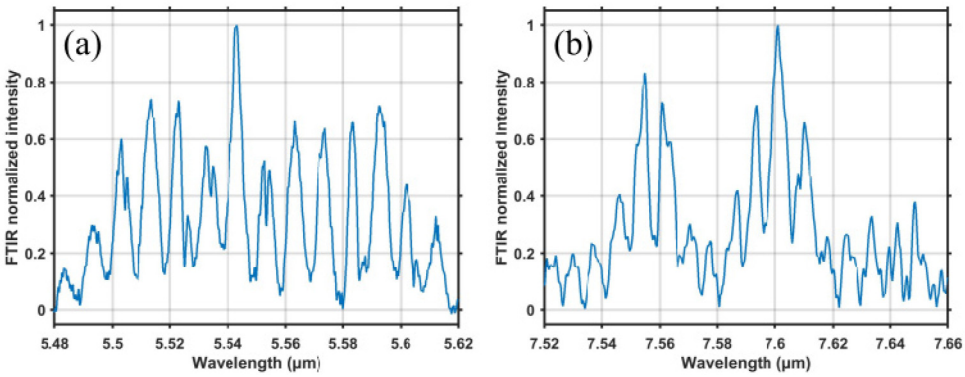

Fig. 7. Measured polarization oscillations at (a) 5.55μm and (b) at 7.55μm. Spectrometer resolution and fiber length are 0.25cm^{-1} and 2.6 m respectively to observe distinct oscillations. Note that the overall transmitted intensity is not constant because of inhomogeneity in the FP-QCL gain profile.

From a Jones matrix analysis, the relationship between the intensity transmission T and the difference between the propagation constants of the polarization axes of the fiber $\Delta\beta = \beta_x - \beta_y$ is given by

$$T \approx \cos^2(\Delta\beta L/2). \tag{3}$$

The phase delay between the two modes at the output of the fiber is equal to $\varphi = \Delta\beta L$ and for a wavelength change $\Delta\lambda$, the differential phase change is [36]

$$\Delta\varphi = L\frac{\partial\Delta\beta(\lambda)}{\partial\lambda}\Delta\lambda = \frac{2\pi L}{\lambda^2}\left[\frac{\partial B(\lambda)}{\partial\lambda} - B(\lambda)\right]\Delta\lambda = -\frac{2\pi L}{\lambda^2}B_g(\lambda)\Delta\lambda. \tag{4}$$

The distance between intensity maxima corresponds to one oscillation period of Eq. (3) and to a phase shift $\Delta\varphi$ of 2π. Using Eq. (4), where λ is the central wavelength between two peaks, the group birefringence is then obtained. The results, shown in Fig. 8(a), are averaged over intervals of 50 nm. The group birefringence at 5.55 μm, 7.55 μm and 8.2 μm are found to be 0.0012, 0.0028 and 0.0036 respectively. Very high birefringence is demonstrated at long wavelength, which permits to preserve polarization at least from 3 to 8.5 μm.

For sake of comparison, the group birefringence B_g can be expressed as $B_g \approx \lambda^k$. The experimental and calculated k values are 2.55 and 2.64, respectively. A very good agreement between the calculated and experimental results is observed. This is because the real geometry of the fiber is implemented in the model, thanks to accurate measurements of every holes diameters and pitch. It validates the optical index of $As_{38}Se_{62}$ obtained from Eq. (1), and, therefore, allows a fine control of polarization properties for future designs. Furthermore, from Eq. (2), the phase birefringence B can be expressed as $B = B_g/(1-k)$. From Fig. 2, it is established that $|B|>|B_g|$ with B and B_g of opposite signs. This inequality is confirmed with value of k greater than 2 and allows to plot the wavelength dependence of phase birefringence in Fig. 8(b). Very good agreement is also observed.

#259359 Received 12 Feb 2016; revised 16 Mar 2016; accepted 21 Mar 2016; published 5 Apr 2016

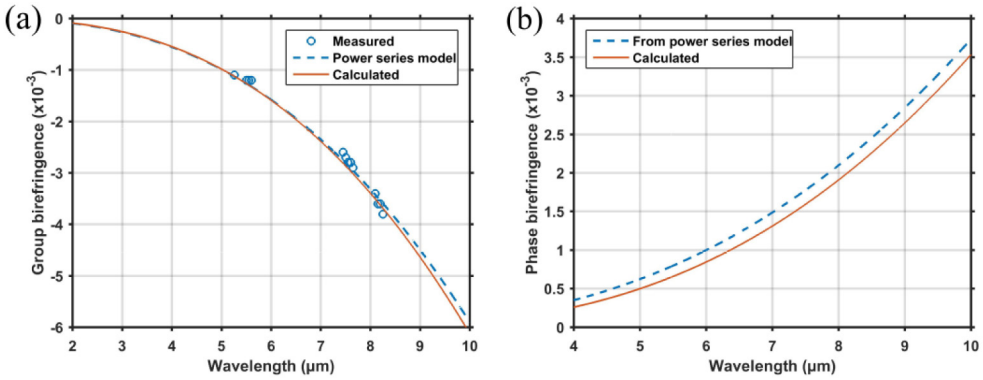

Fig. 8. Wavelength dependence of PM-MOF (a) group birefringence, and (b) phase birefringence. The red solid curve shows the calculated results and the blue shaded curve the fitted results.

5. Conclusion

A single-mode polarization-maintaining MOF covering the mid-IR region from 3 to 8.5 µm is demonstrated for the first time. The $As_{38}Se_{62}$ fiber is composed of three rings of holes with two larger holes in the inner ring and an approximately 9-µm-wide core diameter ensuring single mode operation. Low optical losses (0.8 dB/m) and high group birefringence ($1.5x10^{-3}$) are demonstrated at 7.55 µm. The group birefringence is well accounted for by theoretical calculations. This first experimental demonstration of a chalcogenide birefringent fiber that permits to preserve polarization in the mid-IR, should enable the development of polarization-sensitive sensors.

Acknowledgments

The authors acknowledge the French Délégation Générale pour l'Armement (DGA) and the French Centre National de la Recherche Scientifique (CNRS) for financial supports.

#259359 Received 12 Feb 2016; revised 16 Mar 2016; accepted 21 Mar 2016; published 5 Apr 2016